coatings

MDPI

Article

Improved Uniformity Properties and Corrosion Resistance of Zinc–Nickel Composite Coating Enhanced by Nano-SiO_2

Sujie Chang [1,†], Yuanhao Wang [1,2,†], Jianpeng Wang [3], Zerui Hao [1], Yang Yang [1], Yi Wang [4], Xinyi Wang [1], Fan Cao [1,*] and Lei Shi [1,*]

[1] School of Materials Science and Engineering, Shandong Jianzhu University, Jinan 250101, China; 13771@sdjzu.edu.cn (S.C.); 13270589089@163.com (Y.W.); 15235670840@163.com (Z.H.); 18678652308@163.com (Y.Y.); wang1556243@163.com (X.W.)
[2] Yangzhou Hanshun Automotive Components Co., Ltd., Yangzhou 225000, China
[3] School of Materials and Chemical Engineering, Southwest Forestry University, Kunming 650224, China; ddfdarkholme@126.com
[4] Wendeng Guangrun Metal Products Co., Ltd., Weihai 266440, China; grjswy@126.com
* Correspondence: caofan_success@126.com (F.C.); slcqj@sdjzu.edu.cn (L.S.)
† These authors contributed equally to this work.

Abstract: In this study, pre-treated low-carbon steel substrates were electroplated with Zinc–Nickel (ZN) alloy composite coatings enhanced by the incorporation of nano-silicon dioxide (SiO_2) particles in an alkaline solution. ZN deposits with varying concentrations of nano-SiO_2—specifically, 1, 2, 3, 5, and 10 wt%—were achieved by adjusting the ratio between the nano-SiO_2 and ZN alloy electroplating solutions. The influence of the nano-SiO_2 content on both the quality of the coating and its corrosion behavior was investigated in detail. Scanning electron microscopy (SEM), energy-dispersive spectroscopy (EDS), and an atomic force microscope (AFM) were utilized to assess the surface, cross-section structure, elemental composition, and thickness of the coatings. Notably, the addition of nano-SiO_2 improved the microstructure of the coating, leading to a reduction in grain size as well as enhancements in uniformity and density while revealing that co-deposition reached an optimal concentration at 3 wt% nano-SiO_2. The corrosion behavior of coated specimens was evaluated through electrochemical impedance spectroscopy (EIS) and polarization techniques within a 3.5 wt% NaCl solution serving as a corrosive medium. Specifically, for typical prepared coatings, the corrosion current density decreased from 1.410×10^{-4} A·cm^{-2} to 5.762×10^{-6} A·cm^{-2}, which is a remarkable reduction by one to two orders of magnitude relative to the SiO_2-free coatings mentioned previously. These findings provide a straightforward approach for selecting 3 wt% nano-SiO_2 as an effective additive in ZN composite coatings.

Keywords: zinc–nickel alloy; nano-SiO_2; corrosion resistance; composite coating

Academic Editors: Bassiouny Saleh, Hongyu Wei and Hongwei Shi

Received: 13 December 2024
Revised: 5 January 2025
Accepted: 6 January 2025
Published: 10 January 2025

Citation: Chang, S.; Wang, Y.; Wang, J.; Hao, Z.; Yang, Y.; Wang, Y.; Wang, X.; Cao, F.; Shi, L. Improved Uniformity Properties and Corrosion Resistance of Zinc–Nickel Composite Coating Enhanced by Nano-SiO_2. *Coatings* **2025**, *15*, 71. https://doi.org/10.3390/coatings15010071

1. Introduction

Since the 1990s, electrodeposited zinc alloy coatings have been widely employed to protect steel components from corrosion, with Zn-Fe, Zn-Co, and Zn-Ni alloys being the most prevalent [1–4]. These alloys not only exhibit favorable mechanical properties but also demonstrate superior corrosion resistance compared to pure zinc, positioning them as potential alternatives to cadmium coatings that are now prohibited. Among these options, ZN composite electrodeposits are predominantly utilized as corrosion-protective coatings in the automotive industry [5–10]. ZN composite coatings provide cathodic sacrificial protection for iron and typically offer higher corrosion resistance than both

pure zinc deposits and other zinc alloy coatings; their maximum protective capability is generally achieved at nickel concentrations of up to 25 wt% [2]. Extensive research has explored this topic using both acidic and alkaline plating solutions [2,4,7–17]. Typically, a relatively low nickel content (usually between 4–10 wt%) along with a non-uniform nickel distribution across the coating is observed when electroplated in a weak acid electrolyte bath. In contrast, ZN alloys characterized by more uniform coatings and significantly higher nickel contents are commonly produced in alkaline plating solutions [10,17]. Given the widespread use of low-carbon steel in manufacturing tools intended for long-term operation in strongly alkaline environments, there is an increasing need to identify effective methods for preventing the corrosion of these steels under such conditions.

Although ZN alloy coatings are recognized for their exceptional sacrificial protection and commercial applicability, they tend to lose their protective capabilities when subjected to conditions that induce significant wear and tear [10–17]. Metal corrosion, which is known as a primary cause of surface deterioration, adversely affects the intrinsic properties of materials and structures, including strength, appearance, and permeability. To mitigate this phenomenon, incorporating one or more nanoparticles as effective fillers in alkaline electrolytes or electroless plating can yield multifunctional composite coatings with enhanced self-lubrication, surface hardness, wear resistance, and corrosion resistance; examples include TiO_2, SiC, Al_2O_3, and SiO_2 nanocoatings, and so on [1–14,16–20]. Among these options, nano-SiO_2 has gathered considerable research interest due to its performance in strong acid or alkali baths at ambient temperatures, alongside its inherent high microhardness [21–33]. Furthermore, nano-SiO_2 is both cost-effective and readily available. However, from the perspective of oil–water separation principles, the hydrophobicity of nano-SiO_2 poses challenges for blending it with metal matrices. Fortunately, Tu et al. reported that the unsaturated oxygen bonds on the surface of nano-SiO_2 particles can capture some absorbed nickel atoms, forming nickel–oxygen bonds [34]. Various researchers have employed different strategies to modify nano-SiO_2 particles, such as incorporating dispersants or other additives into the electrolyte [34–37]. Hou et al. demonstrated that modified nano-SiO_2 was achieved using a hybrid medium of fluoro-epoxy polymer [35]. Similarly, Xiong et al. indicated that KH-550-modified nano-SiO_2 particles were utilized to enhance the compatibility between melamine-formaldehyde prepolymer and polyvinyl alcohol (PVA). Additionally, Hu et al. noted that triethanolamine (TEA) is commonly used as a grinding aid [37]; they modified graphene oxide with TEA to reduce aggregation in pore solutions. Given the abundance of hydroxyl (-OH) groups in TEA, it effectively prevents deoxygenation in highly alkaline solutions while maintaining hydrophilicity. This study aimed to utilize TEA primarily as a complexing agent since its ability to bind with hydroxyl groups facilitates improved interaction between nano-SiO_2 and electrolytes.

In this study, composite electrodeposition was employed to successfully prepare Zn-Ni-SiO_2 composite coatings using commercial nano-SiO_2 particles at varying dosages on low-carbon steel at ambient temperature. Subsequently, the nanoparticles were incorporated into the plating bath to fabricate coatings via the electrodeposition method with the assistance of TEA. The surface morphology and structural composition of the as-prepared coatings were analyzed using field emission scanning electron microscopy (FESEM) (TISKEN (China) Co., Ltd., Brno, Czech Republic) coupled with energy-dispersive spectroscopy (EDS) (Oxford Instrument Technology (Shanghai) Co., Ltd., Shanghai, China), as well as atomic force microscopy (AFM) (Oxford Instrument Technology (Shanghai) Co., Ltd., Shanghai, China). Additionally, the corrosion resistance of these coatings was evaluated through electrochemical measurements [38].

Herein, the objective of the recent work was to investigate the influence of nano-SiO_2 content on the corrosion behavior of electrodeposited ZN alloy coatings, with a primary

focus on the evolution of surface and cross-sectional morphology, elemental composition, thickness, and corrosion resistance. Additionally, the potentiodynamic polarization behavior of the coatings was examined as corrosion progressed. Furthermore, the long-term corrosion behavior of the tested specimens was assessed in terms of corrosion depth.

2. Materials and Methods

2.1. Chemicals and Reagents

All chemicals used in the experiment are analytically pure, including NaOH (Tianjin Hengxing Chemical reagent Manufacturing Co., Ltd., Tianjin, China), ZnO (analytically pure, Tianjin Damao chemical reagent factory, Tianjin, China), $NiSO_4 \cdot 6H_2O$ (analytically pure, Xilong Scientific Co., Ltd., Shantou, China), triethanolamine (TEA, analytically pure, Tianjin Fuyu Fine Chemical Co., Ltd., Tianjin, China), DPE-III (analytical purity, Guangzhou Second Light Industry Research Institute, Guangzhou, China), BH-336 (analytical purity, Guangzhou Second Light Industry Research Institute, Guangzhou, China), NaCl (analytical purity, China National Pharmaceutical Group Chemical Reagent Co., Ltd., Shanghai, China), HCl (analytical purity, China National Pharmaceutical Group Chemical Reagent Co., Ltd., Shanghai, China), HNO_3 (analytical purity, China National Pharmaceutical Group Chemical Reagent Co., Ltd., Shanghai, China), conventional stabilizer (analytical purity, Guangzhou Second Light Industry Research Institute, Guangzhou, China), and deionized water (DI water). The average diameter of nano-SiO_2 is 20 nm, and it was purchased from Shanghai Yaoyi Alloy Materials Co., Ltd., Shanghai, China, providing the details of particle properties. ZN alloy coatings were prepared by electrodeposition from an alkaline TEA bath, and all the reagents were used as received without any further purification. Commercial Q235 low-carbon steel sheets were used as the substrate.

2.2. Electrolyte Preparation

Electrolytes were prepared using ZnO (8–12 g/L), NaOH (130–140 g/L), $NiSO_4 \cdot 6H_2O$ (4–8 g/L), TEA (28–30 g/L), stabilizer (8–12 g/L), DPE-III (5–10 mL/L), and BH-336 (2–6 mL/L). Among them, DPE-III serves as the principal brightener in the alkaline electroplating ZN alloy, comprising primarily dimethylaminopropylamine. BH-336, on the other hand, functions as the secondary brightener, encompassing a carrier brightener, main brightener, auxiliary brightener, wetting agent, and impurity removal agent [5]. The weighed NaOH and ZnO are completely dissolved after stirring in distilled water and placed in the same beaker. After $NiSO_4 \cdot 6H_2O$ was stirred and clarified, TEA was added to form a stable complex with Ni^{2+} ions, and a stabilizer was added after complexation to make the plating solution stable [39]. Finally, DPE-III and BH-336 were poured into the reagent sequentially.

After polishing and cleaning the cathode for electrode deposition, it is essential to ensure the proper adhesion of the coating to the substrate. In order to prepare coatings with different nano-SiO_2 concentrations, laboratory-scale plating was carried out using a vertical plating bath. The anode and cathode are made of a nickel sheet and thoroughly degreased low-carbon steel plate (60 mm × 40 mm × 0.8 mm), at a current density of 4 A/cm^2 and a room temperature of 25 ± 2 °C. Before electroplating, the low-carbon steel sheet is polished with 400#, 800#, and 1000# sandpaper, successively. Then, it is cleaned thoroughly with anhydrous ethanol, acetone, and DI water for 3 min, respectively. The DC rectifier was used for electrodeposition for 15 min. The compositions, parameters selection, and plating conditions are listed in Table 1. For the electroplating of ZN composite coating, different concentrations of nano-SiO_2 (1 wt–10 wt%) were adjusted by changing the concentration added to the prepared alkaline electrolytes until uniform dispersion at room temperature. Based on the final measured silica content, herein, various ZN

composite coatings with nano-SiO_2 are denoted, including pure ZN alloy, ZN-1wt%SiO_2, ZN-2wt%SiO_2, ZN-3wt%SiO_2, ZN-5wt%SiO_2, and ZN-10wt%SiO_2, respectively. In all these samples, the content of Ni is between 12% and 14%.

Table 1. Composition, parameter selection, and plating conditions for electrodeposition of ZN alloys.

Composition and Parameter Selection	Concentration and Parameter Value	Electrodeposition Parameters
NaOH (g/L)	130–140	pH 12.0
ZnO (g/L)	8–12	Temperature 25 ± 2 °C
$NiSO_4 \cdot 6H_2O$ (g/L)	4–8	Planting time 15 min
TEA (g/L) DPE-III (ml/L) BH-336	28–30 5–10 2–6	Stirring speed 120 rpm Current density 4 A/dm^2
Stabilizer (g/L)	8–12	-

2.3. Structural Analysis of Electroplated Coatings

The surface microstructure and roughness of the prepared samples under an acceleration voltage of 5–10 kV were observed using a Zeiss Ultra™55 scanning electron microscope (SEM) and secondary electron signal. The chemical composition of the coating was analyzed using Energy-Dispersive Spectroscopy (EDS) based on scanning electron microscopy, and the EDS results were semi-quantitative. An Asylum Research Cypher S atomic force microscope (AFM) was employed to inspect the surface topography and roughness of the samples. The samples were placed on a sample holder.

2.4. Electrochemical Tests

According to ASTM G5-14 and ASTM G106-89 standards [40,41], the prepared samples were tested using Tafel curves (Tafel) and measured by electrochemical impedance spectroscopy (EIS) using a Shanghai Chenhua CHI760E electrochemical workstation (Shanghai chenhua Instrument Co., Ltd., Shanghai, China) at 25 ± 2 °C. Among them, a standard three-electrode system was used, in which a 1 cm^2 sample was used as the working electrode, the platinum electrode (Pt) as the auxiliary electrode, and the saturated calomel electrode as the reference electrode. The open circuit potential was monitored for 10 min. All electrochemical tests were performed in a 3.5 wt% NaCl solution, and the EIS was measured at frequencies ranging from 10^5 Hz to 10^{-1} Hz, with a signal amplitude set to 5 mV. Following EIS measurements, dynamic potential polarization (Tafel) tests were performed at a rate of 1 mV/s. In order to ensure the accuracy of the test, EIS measurement is performed first to avoid the influence of the Tafel test on the surface state of the sample. In addition, all experiments were repeated to ensure the repeatability and reliability of the results. Through these detailed tests, the corrosion resistance of different coatings was evaluated; thus, a scientific basis was provided for optimizing the plating process. The calculation of the electrochemical corrosion rate is based on Faraday's law, which states that in electrochemical reactions, the amount of charge passing through the electrodes Q is proportional to the number of electrons transferred *n*, and the proportionality constant is the Faraday constant F. By measuring the corrosion current icorr, which is the flow of electric charge through the electrode per unit time, the formula $R_{corr} = \frac{i_{corr} \times E_w}{A \times d}$ is used to calculate the corrosion rate. Among them, icorr is the corrosion current density, Ew is the equivalent weight, A is the surface area, and d is the material density. This formula reflects the direct relationship between the corrosion rate and the charge transfer in the

electrochemical reaction, allowing for the quantitative evaluation of the corrosion loss of materials from electrochemical measurements.

2.5. Salt Spray Test Conditions

Salt spray tests were conducted to evaluate the long-term corrosion resistance of ZN-SiO_2 composite coatings, in accordance with ASTM B117 standards [42]. The test was performed in a salt spray chamber maintained at a temperature of 35 ± 2 °C, with a 5 wt% NaCl solution atomized to create a highly corrosive environment. Coated samples were positioned at an angle of 15–30° relative to the horizontal plane to ensure uniform exposure to the saline fog, during which the specimens were periodically inspected for visible signs of corrosion, such as rust formation or coating delamination. The performance of the coatings was assessed based on the extent of surface degradation and the time to the onset of substrate corrosion. This test provided critical insights into the durability of the coatings under simulated marine conditions.

3. Results and Discussion

3.1. Surface Morphology and Elemental Composition

The components used in composite electroplating significantly influence the surface morphology and uniformity of the coatings [11,12,16]. The microscopic surface morphology of ZN composite coatings with varying nano-SiO_2 contents at magnifications of 5 k and 10 k is illustrated in Figure 1. For pure ZN alloy coatings, as shown in Figure 1(a1), numerous irregular particles (dashed circles) are present, resulting in a rough and dull appearance on the surfaces. In Figure 1(a2)), distinct micro-pores (square frames) are particularly evident. Some literature reports suggest that these micro-pores may originate from the release of absorbed hydrogen atoms from the substrate during the plating process [9,19]. Notably, no significant peak for silicon (Si) is observed in the EDS spectrum presented in Figure 1(a3). Upon adding nano-SiO_2, a marked transformation in surface morphology was noted at ZN-3wt%SiO_2; specifically, very flat and smooth surfaces were observed. As depicted in Figure 1(b1), the surface roughness diminished completely at this concentration, which shows an orderly arrangement devoid of defects such as micro-pores or impurities and indicates that ZN-3wt%SiO_2 achieved a more uniformly distributed coating during electroplating. At higher magnification (10 K), grain refinement compared to pure ZN composite coatings is evident (Figure 1(b2)). This figure illustrates that the coatings are uniform and compact while fully covering the substrates; however, the Si content remains negligible according to EDS analysis (Figure 1(b3)). Along with an increase to a SiO_2 concentration of 5 wt%, Figure 1(c1) reveals some nodular grains (triangular frames) on the coating's surface while maintaining overall flatness, which suggests that increased surface roughness correlates with a higher nano-SiO_2 content. At greater magnification (Figure 1(c2)), differences in the particle size become more pronounced; yet, the EDS patterns indicate no significant increase in Si peaks compared to the samples with a concentration of 3 wt% nano-SiO_2 (Figure 1(c3)).

As the concentration of nano-SiO_2 increases to 10 wt%, the electroplating specimen image is presented in Figure 2. Figure 2a reveals a relatively rough and uneven surface texture. At higher magnification (Figure 2b), a significant number of particles and inconsistencies in the coating become more apparent. The elevated concentration of nano-SiO_2 hinders uniform dispersion within the electroplating solution, leading to an increased likelihood of self-aggregation during the plating process, which results in larger particles adhering to the coating's surface and contributing to surface roughness, as well as the emergence of nodular grains and hairline cracks. The presence of these grains and cracks on the

coating can primarily be attributed to internal stress; specifically, large tensile stresses are particularly detrimental, significantly accelerating crack formation [16].

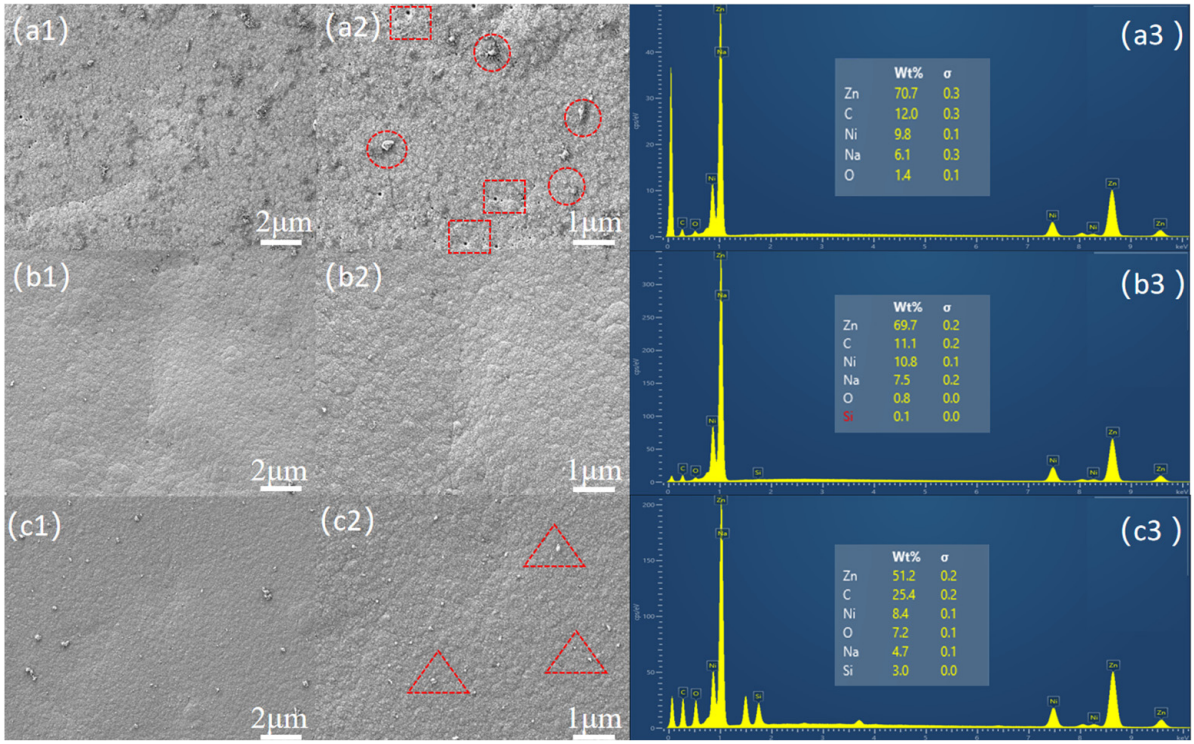

Figure 1. SEM micrographs of the surface of ZN alloy coatings with different nano-SiO_2 contents at various magnifications: (**a1**–**a3**) no SiO_2, (**b1**–**b3**) 3 wt%, and (**c1**–**c3**) 5 wt%. (**a1**,**b1**,**c1**): 5000× (**a2**,**b2**,**c2**): 10,000×. (**a3**,**b3**,**c3**) EDS measurement and analysis diagram of electroplate coatings. Square frames (**a2**) highlight micro-pores, dashed circles (**a2**) indicate irregular particles, and triangular frames (**c2**) mark nodular grains.

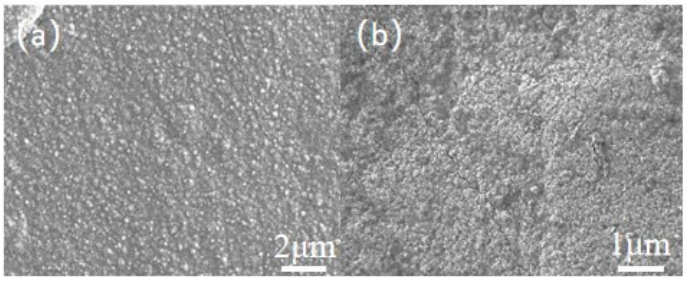

Figure 2. (**a**,**b**) SEM images of the ZN-10 wt% nano-SiO_2 at different magnifications. (**a**): 5000×; (**b**): 10,000×.

When the concentration of nano-SiO_2 exceeds 5 wt%, particle agglomeration and the formation of micro-cracks in the coating are observed, negatively impacting the uniformity and performance of the coating. To address these challenges, potential strategies include the surface modification of nano-SiO_2 using silane coupling agents, the introduction of dispersants such as PVA into the electroplating solution, and the application of ultrasonic agitation during the electrodeposition process. These methods aim to enhance the dispersibility of nanoparticles and will be further explored in future research to optimize the performance of the coating.

To further investigate the distribution within the composite coatings, EDS mappings of ZN coatings with nano-SiO_2 are presented in Figure 3. It can be observed in Figure 3 that the ZN-3wt%SiO_2 coating exhibits uniform distribution; specifically, the intensities of zinc

(Zn), nickel (Ni), carbon (C), silicon (Si), and oxygen (O) elements are evenly distributed throughout the matrix, aligning with the results shown in Figure 1(b3). The presence of Si and O corresponds to the SiO_2 incorporated into the ZN composite coating. Notably, although the measured Si content is quite low, the influence of nano-SiO_2 is significant, which results in enhanced surface flatness, uniformity, and compactness. In contrast, agglomerated SiO_2 particles on the surface of the ZN-10 wt% specimen are clearly visible in Figure 3. The EDS elemental distribution for Si and O also indicates that nano-SiO_2 particles become concentrated in the outer surface region when present at excessive levels within ZN composite coatings. This accumulation of nano-SiO_2 particles at the surface is attributed to some particles adhering to it during electrodeposition after the completion of the plating [26]. Consequently, higher concentrations of nano-SiO_2 in the plating bath lead to rougher and more uneven electroplating coatings, consistent with the observations made in Figure 1.

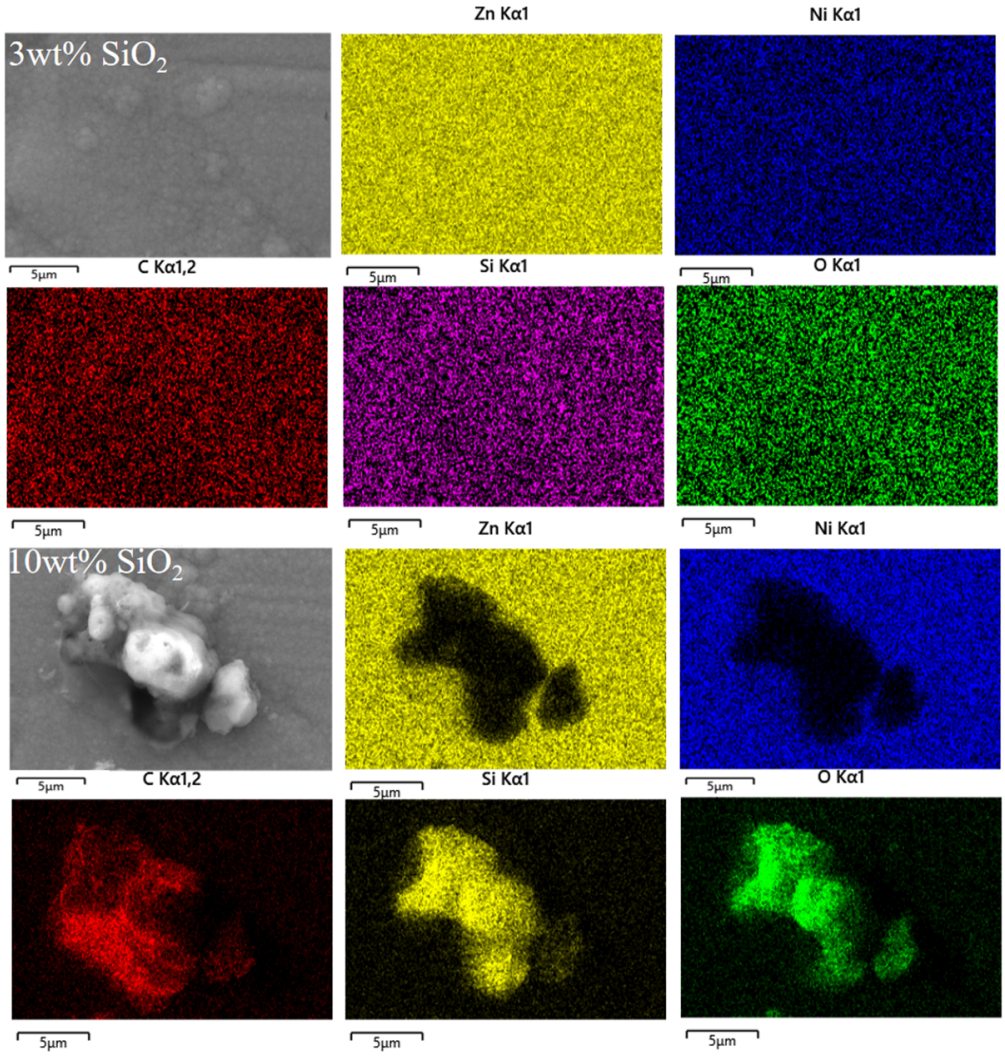

Figure 3. The morphologies and EDS elemental distribution of ZN alloy with 3 wt% and 10 wt% nano-SiO_2, respectively.

3.2. Cross-Section Morphology and Coating Thickness

Additionally, the interface between the coating and substrate at varying nano-SiO_2 concentrations is illustrated by the cross-sectional morphologies in Figure 4. It is evident that the cross-sections of ZN composite coatings with different amounts of nano-SiO_2 exhibit distinct characteristics when compared to low-carbon steel. First, the thickness

of the ZN coating without any added nano-SiO_2 measures 4.42 µm (Figure 4a), which is relatively thinner than that reported in previous literature [31]. The overcoat layers are rough, and pronounced cracks are visible on the surface. Upon adding 3 wt% nano-SiO_2 (Figure 4b), there is minimal change in the thickness, which measures approximately 4.42 µm; yet, cracks have disappeared, resulting in a more condensed crystal structure that appears uniform. As the concentration of nano-SiO_2 increases further, significant voids and finer grains become apparent in the cross-section compared to that of the 3 wt% specimen (Figure 5c). When increasing to a concentration of 5 wt%, a more pronounced interface between particles and substrate emerges; this particle accumulation may contribute to increased local roughness, reflecting interactions between nano-SiO_2 and the substrate [18].

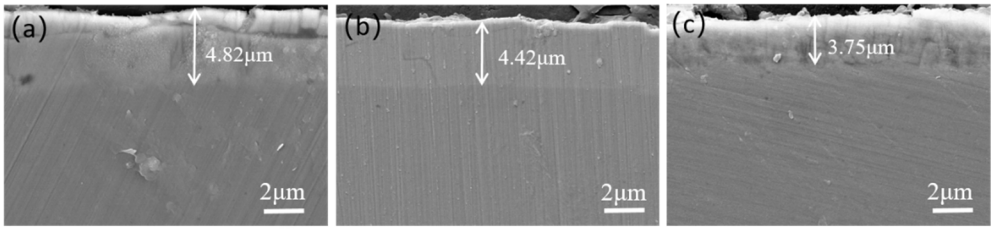

Figure 4. SEM images of the cross-section of the ZN electrodeposits with different nano-SiO_2 contents: (**a**) no SiO_2, (**b**) 3 wt%, and (**c**) 5 wt%.

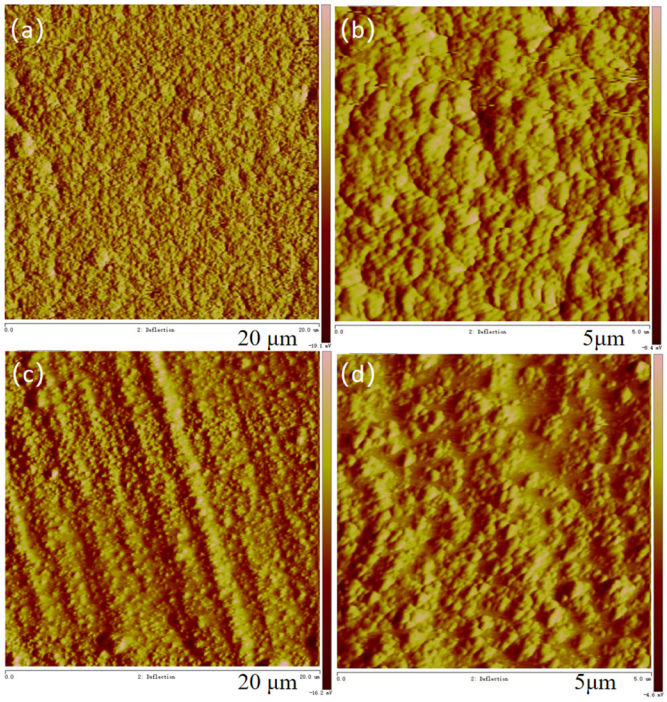

Figure 5. AFM diagram of ZN-3wt%SiO_2 coatings at different microscopic scales: (**a**) AFM diagram of coating at 20 µm scale, (**b**) AFM diagram of coating at 5 µm scale, AFM diagram of ZN-5wt%SiO_2 coatings at different microscopic scales, (**c**) AFM diagram of coating at 20 µm scale, and (**d**) AFM diagram of coating at 5 µm scale.

Based on the findings, the surface quality of the specimen is optimized at a constant current density of 4 $A{\cdot}dm^{-2}$ in an alkaline TEA plating solution containing 3 wt% nano-SiO_2. Additionally, atomic force microscopy (AFM) was employed to analyze the surface topographies of ZN alloy coatings with varying concentrations of nano-SiO_2, as illustrated in Figure 5a–d. These images elucidate how different parameters related to the nano-SiO_2 concentration influence the surface structure of ZN composite coatings. Surface topography investigations conducted over a scanned area of 20 µm × 20 µm reveal notable uniformity

and distribution within the coating (Figure 5a). In Figure 5b (5 μm × 5 μm scale), medium-scale imaging demonstrates that the entire surface of ZN-3 wt% composite coatings exhibits enhanced homogeneity and finer grain structures; this observation suggests a denser particle distribution and greater uniformity in particle size. Conversely, Figure 5c illustrates the surface morphology for samples with a concentration of 5 wt%, where plated coatings are characterized by agglomerated nano-sized granular crystallites. The roughness observed in these regions is significantly elevated, indicating potential particle aggregation or uneven dispersion phenomena. Finally, Figure 5d (also at a scale of 5 μm × 5 μm) provides detailed insights into individual nanoparticles' shapes and sizes along with their contributions to overall surface roughness; at this magnification, there is an observable increase in lattice imperfections compared to specimens with lower concentrations. Therefore, AFM analysis conclusively demonstrates that increasing concentrations of nano-SiO_2 correlate positively with increased surface roughness within ZN composite coatings.

3.3. Electrochemical Corrosion Performance of ZN-SiO_2 Composite Coating

Impedance measurement is widely utilized due to its nondestructive nature. In this study, the corrosion resistance of the as-prepared coatings was further evaluated using electrochemical EIS curves. Figure 6 presents the Nyquist plots of the obtained specimens immersed in a 3.5 wt% NaCl solution, where Z' and Z'' represent the real and imaginary components of measured impedance, respectively. The inset figure highlights an amplified view of the high-frequency range. The presence of a semicircular feature in the impedance curve indicates a capacitive loop, with polarization resistance showing an upward trend, as indicated by an expanding semicircle diameter [5,10,29]. The loop observed at higher frequencies is associated with ionic double-layer capacitance and rapid Faradaic charge transfer processes. Conversely, the loop at lower frequencies may be attributed to responses from exposed fresh substrate areas due to corrosion occurring at the interface between the substrate and coatings [10,21,30,31]. It was observed that as corrosion progressed, the presence of nano-SiO_2 at the ZN/steel interface became increasingly significant.

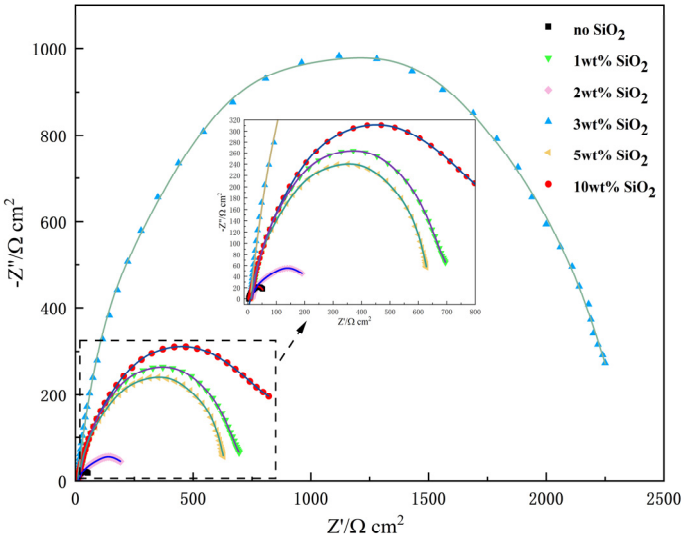

Figure 6. The Nyquist plots of ZN alloy coatings with variable nano-SiO_2 measured in 3.5 wt% NaCl solution. The inset figure is the amplified diagram of the high-frequency range.

All curves demonstrate pronounced passivation behavior within a similar potential range, indicating that the corrosion current remains relatively constant as the potential increases. This passivation behavior suggests the formation of a protective passivation film under these conditions. As the concentration of nano-SiO_2 further increases, it is

observed that the passivation region widens, which is particularly evident in the curve for the 3 wt% specimen. Generally, a larger radius of the loop correlates with the improved corrosion resistance of the coating [6,10,21,31]. The relationship between the semicircle diameter and corrosion resistance has garnered significant attention. With increasing concentrations of nano-SiO_2, there is a corresponding decrease in corrosion current, suggesting that incorporating nano-SiO_2 enhances the corrosion resistance of ZN composite coatings. The ZN-3wt%SiO_2 coating exhibits a greater arc radius and consequently demonstrates superior corrosion resistance. However, it is noteworthy that some curves display shifts in corrosion potential; this may indicate that higher concentrations of nano-SiO_2 influence the passivation behavior of the metal surface. These changes could be related to microstructural modifications induced by nano-SiO_2 on coating surfaces. All curves demonstrate pronounced passivation behavior within a similar potential range, indicating that the corrosion current remains relatively constant as the potential increases.

From Bode plots of the impedance module in Figure 7, the ZN-3wt%SiO_2 coating shows the largest module value in the low-frequency domain, suggesting enhanced anti-corrosion. As mentioned above, a thin passivation layer protected the ZN alloy from corrosion.

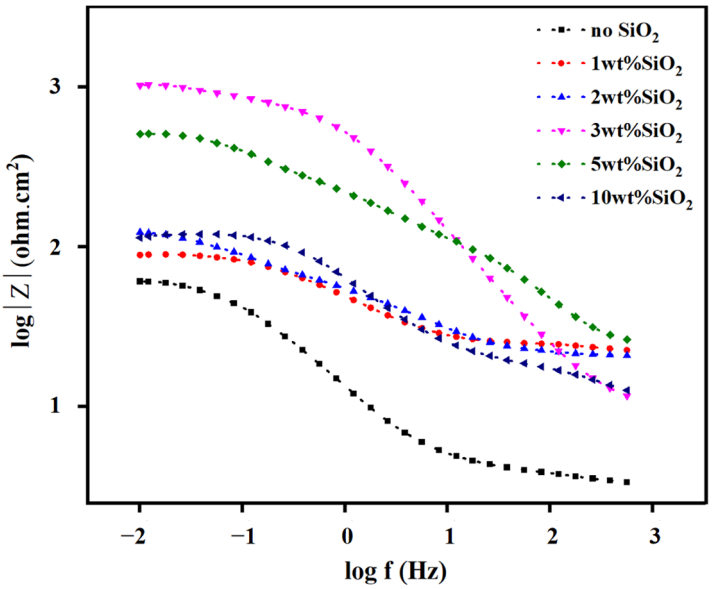

Figure 7. Bode plots obtained for ZN alloy coatings with various nano-SiO_2.

The equivalent circuit model for impedance fitting is illustrated in Figure 8, comprising solution resistance (Rs), charge transfer resistance (Rct), polarization resistance (Rp), also referred to as charge transfer resistance, and constant phase elements (CPE), which reflect kinetic corrosion parameters [10]. This circuit facilitates the simulation of the solution/coating interface and enables Nyquist plot analysis. Notably, a higher Rp value indicates an enhancement in corrosion resistance within the coating [5]. The values of Rp are summarized in Table 2; a systematic analysis of the concentration variations of nano-SiO_2 in ZN composite coatings was performed to evaluate its influence on the Rp of these coatings. Experimental data revealed a nonlinear relationship between the SiO_2 concentration and Rp. In the absence of SiO_2, the measured Rp was 68.07 $\Omega \cdot cm^2$. As the nano-SiO_2 concentration gradually increased to 1 wt%, a modest rise in Rp to 74.35 $\Omega \cdot cm^2$ was observed, suggesting that incorporating nano-SiO_2 had an initial positive effect on coating resistance. At a nano-SiO_2 concentration of 3 wt%, however, the Rp value surged to 2282 $\Omega \cdot cm^2$, indicating that this level may represent an optimal addition of nano-SiO_2 into the coating, enhancing its uniformity and compactness while consequently improving corrosion resistance.

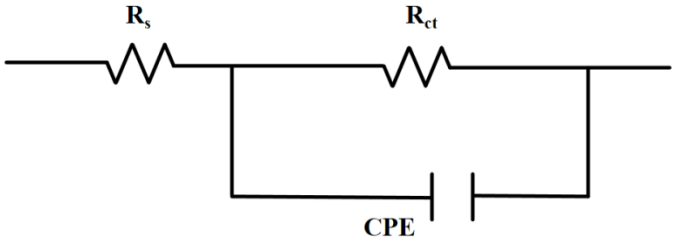

Figure 8. The equivalent circuit model of impedance diagrams fitting.

Table 2. Rp of ZN alloy coatings with different nano-SiO_2 concentrations calculated based on the equivalent circuit diagram.

ZN Alloys Coatings	Rp ($\Omega \cdot cm^2$)
no SiO_2	68.07
1% SiO_2	74.35
2% SiO_2	131.4
3% SiO_2	2282
5% SiO_2	117.7
10% SiO_2	110.4

However, as the SiO_2 concentration continues to rise, the Rp value begins to decline, indicating that once the optimal concentration is surpassed, further increases in SiO_2 may not yield a beneficial effect on resistance. Instead, the excessive aggregation of nano-SiO_2 within the coating could lead to diminished resistance performance. Consequently, this parameter's optimized value has been identified as 3 wt%.

The Tafel polarization potentiodynamic curves for ZN composite coatings with varying concentrations of nano-SiO_2 are depicted in Figure 9. Table 3 delineates the effects of alterations in the nano-SiO_2 content on the polarization results derived from Tafel curve analysis, which yields electrochemical parameters and corrosion rates for selected specimens. The observed curves demonstrate that the corrosion potential of ZN composite coatings incorporating nano-SiO_2 shifts to more positive values compared to those without, while the corrosion current decreases, indicating that the incorporation of nano-SiO_2 has significantly enhanced corrosion performance (Table 3). This enhancement is attributed to the role of nano-SiO_2 particles within the coating matrix, which increases charge transfer resistance during the corrosion process, thereby improving overall corrosion resistance. Notably, at a concentration of 3 wt% nano-SiO_2, both the stability and protective efficacy of the passivation film are markedly improved. However, it is important to note that higher concentrations of nano-SiO_2 may lead to an increase in current density within low potential regions on the polarization curve; this could suggest potential issues related to coating integrity due to excessive amounts of nano-SiO_2 or the localized acceleration of corrosive reactions.

In Table 3, the corrosion potentials for all tested coatings remain negative relative to the low-carbon steel substrate, indicating that each of these coatings offers a degree of galvanic or sacrificial protection to the steel substrate. More importantly, the corrosion current density (icorr) serves as a critical parameter in evaluating corrosion performance. Notably, the icorr of the ZN composite coating with 3 wt% nano-SiO_2 (5.762×10^{-6} $A \cdot cm^{-2}$) is significantly lower than that of the pure ZN alloy coating without nano-SiO_2 addition, exhibiting reductions in the order of one to two magnitudes. The result is similar to Xiang's report on Zn-Ni-SiO_2 coating and the coating with ceria-modified SiO_2 [31]. This decrease in corrosion current density corresponds with an enhancement in the anti-corrosion properties of the ZN composite coating. Furthermore, there is a direct correlation between the corrosion rate and corrosion current density, providing a more intuitive measure of

anti-corrosion performance. The corrosion rate for pure ZN alloy coating is recorded at 1.23×10^{-5} g·m^{-2}·h^{-1}; however, upon incorporating nano-SiO_2 into the electroplating bath, this rate decreases notably for specimens containing nano-SiO_2, particularly those at 3 wt% (0.58×10^{-5} g·m^{-2}·h^{-1}). Consequently, these specimens exhibit relatively higher levels of corrosion resistance associated with their smoother surface.

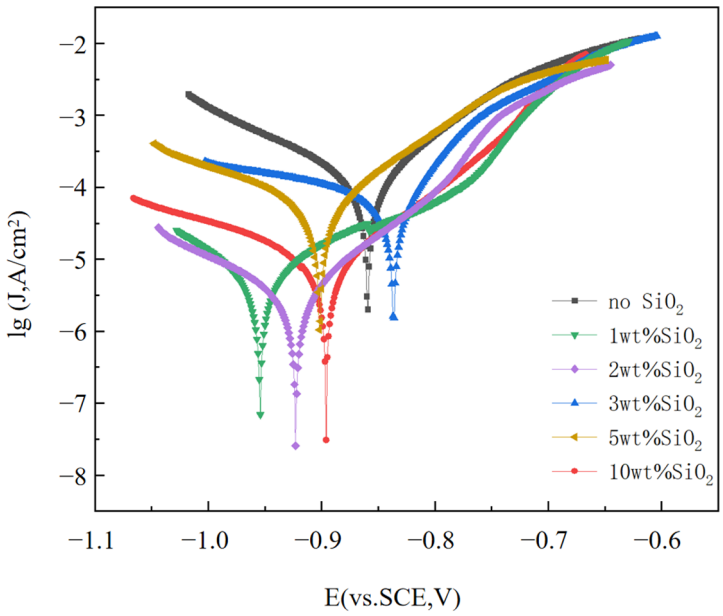

Figure 9. Tafel curves with different concentrations of nano-SiO_2 were added.

Table 3. The electrochemical parameters (Ecorr, icorr) extracted from the Nyquist plots and corrosion rates of partial specimens.

Samples	Ecorr (V)	Icorr (A/cm^2)	Corrosion Rate (10^{-5} g·m^{-2}·h^{-1})	Anodic Slope (mv/Decade)	Cathodic Slope (mv/Decade)
no SiO_2	−0.8582	1.410×10^{-4}	1.23	7.057	11.105
1% SiO_2	−0.9126	4.929×10^{-5}	-	4.560	13.842
2% SiO_2	−0.9214	6.761×10^{-5}	-	7.642	11.584
3% SiO_2	−0.9549	5.762×10^{-6}	0.58	5.229	4.800
5% SiO_2	−0.8872	1.100×10^{-4}	0.96	2.897	9.611
10% SiO_2	−0.8914	4.676×10^{-5}	-	2.962	9.742

Accordingly, the data from these polarization curves elucidate the impact of nano-SiO_2 on the corrosion resistance of ZN composite coatings. The incorporation of nano-SiO_2 at an optimal concentration can significantly enhance the coating's corrosion resistance. In summary, the polarization curve analysis indicates that adding nano-SiO_2 contributes to a marked improvement in the corrosion resistance of ZN alloy coatings.

3.4. Long-Term Corrosion Resistance Assessment

To further verify the long-term corrosion resistance of the ZN-SiO_2 composite coating, a salt spray test was conducted. The results in Table 4 indicate that the ZN coating containing 3 wt% nano-SiO_2 exhibits superior corrosion resistance compared to both the ZN coating without nano-SiO_2 and the coating with a higher concentration of nano-SiO_2.

Table 4. The time for 5% red rust to appear on ZN alloy coatings at different concentrations.

Type of Coating	Time to 5% Red Rust (Hours)
no SiO_2	216
3% SiO_2	384
5% SiO_2	336

Specifically, a 3 wt% nano-SiO_2 coating exhibited the best corrosion resistance. In contrast, coatings without nano-SiO_2 or with higher SiO_2 concentrations demonstrated localized corrosion and delamination of the coating. These findings align with the electrochemical impedance spectroscopy and Tafel analysis we provided, confirming that a 3 wt% nano-SiO_2 concentration optimally enhances the uniformity and compactness of the coating, thereby improving its ability to withstand prolonged exposure in corrosive environments.

The results of the salt spray test corroborated the previously provided electrochemical data and demonstrated the stability of the proposed coating under marine or industrial-like conditions. This long-term performance further underscores the potential industrial applications of the ZN composite coating with an optimal nano-SiO_2 content.

3.5. Possible Reaction Model

Based on the aforementioned experimental results, a schematic model illustrating the variable applications of electrodeposited ZN-SiO_2 composite coatings is presented in Scheme 1. In the study, low-carbon steel served as the substrate; however, conventional ZN plating solutions often lead to surface micro-pores and irregular particles within the coating. The incorporation of nano-SiO_2 significantly influences the nucleation and growth processes, composition, and microstructure of ZN composite coatings. An optimal addition level of 3 wt% nano-SiO_2 was identified. Compared to pure ZN alloy coatings, the ZN-SiO_2 nanocomposite coatings exhibit flatter and smoother surfaces along with markedly improved corrosion resistance. However, an increase in nano-SiO_2 content leads to the self-aggregation of nanoparticles on the surface. Consequently, these aggregated nanoparticle clusters can obstruct vacant areas on the surface and hinder further growth. This elucidates the mechanism by which corrosion resistance is enhanced in ZN composite coatings within an alkaline bath through a synergistic effect between nano-SiO_2 and TEA used as complexing agents. The work provides significant application value for enhancing corrosion resistance in ZN composite coatings while underscoring potential advantages related to additive amounts of nano-SiO_2.

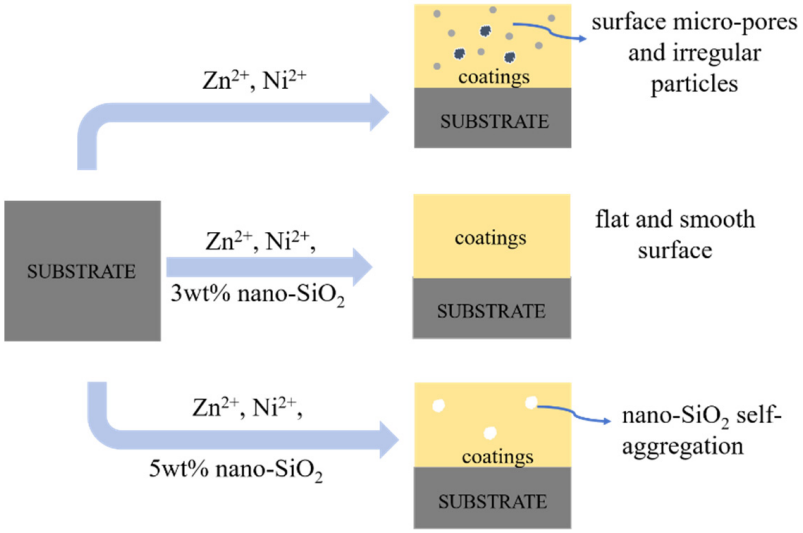

Scheme 1. A schematic model of the variable applications of electrodeposited ZN alloy coatings.

4. Conclusions

This study investigates the effect of nano-SiO_2 on the corrosion resistance of ZN composite coatings. Different concentrations of nano-SiO_2 were added to the ZN alkaline TEA plating solution, and electroplating was performed at a consistent current density of 4 A/dm^2. Based on comprehensive test results and EDS analysis, it is concluded that an optimal additive dosage of nano-SiO_2 is 3 wt%. The influence of these nanoparticles on the microstructure, uniformity, and densification of the coating was examined. The results from SEM and AFM surface morphology analyses further confirmed that the dispersion of nano-SiO_2 in the plating solution significantly affects coating quality. Through analyses using EIS, Tafel curves, and corrosion current density measurements, the mechanism by which corrosion resistance is enhanced in these coatings is elucidated. Notably, adding 3 wt% nano-SiO_2 improved both electrochemical stability and corrosion resistance compared to conventional coatings; this enhancement arises from a uniform distribution of nanoparticles within the coating matrix. Additionally, variations in Si peak values corroborate changes in thickness and uniformity directly related to coating corrosion resistance.

This study offers a novel perspective on enhancing the corrosion resistance of ZN alloy coatings and highlights the potential advantages of incorporating nano-SiO_2, which presents significant application prospects in the industrial electroplating sector. Correspondingly, it can be foreseen that compared with traditional commercially available ZN alloys, ZN composite alloys with appropriate amounts of nano-SiO_2 will have better corrosion resistance.

Author Contributions: Conceptualization, S.C. and F.C.; Methodology, S.C., Y.W. (Yuanhao Wang), X.W. and L.S.; Software, J.W.; Validation, S.C., Y.W. (Yuanhao Wang), J.W., Z.H., Y.Y. and Y.W. (Yi Wang); Formal analysis, X.W.; Data curation, S.C., Y.W. (Yuanhao Wang), J.W., Y.W. (Yi Wang), X.W. and F.C.; Writing – original draft, J.W.; Writing – review & editing, S.C.; Project administration, S.C., F.C. and L.S.; Funding acquisition, S.C., F.C. and L.S. All authors have read and agreed to the published version of the manuscript.

Funding: This work was financially supported by the 2018 Doctoral Research Funds of Shandong Jianzhu University (X18064Z) and the Joint Fund Project for Natural Science Foundation of Shandong Province (ZR202108100033).

Institutional Review Board Statement: Not applicable.

Informed Consent Statement: Not applicable.

Data Availability Statement: The data presented in this study are available in this article.

Acknowledgments: The authors want to thank the Jinan Institute of Quantum Technology for their assistance with the AFM measurements.

Conflicts of Interest: Author Yuanhao Wang was employed by the Yangzhou Hanshun Automotive Components Co., Ltd. Author Yi Wang was employed by the Wendeng Guangrun Metal Products Co., Ltd. The remaining authors declare that the research was conducted in the absence of any commercial or financial relationships that could be construed as a potential conflict of interest.

References

1. Crotty, D. Zinc Alloy Plating for the Automotive Industry. *Met. Finish.* **1996**, *94*, 54–58. [CrossRef]
2. Baldwin, K.R.; Robinson, M.J.; Smith, C.J.E. The Corrosion Resistance of Electrodeposited Zinc-Nickel Alloy Coatings. *Corros. Sci.* **1993**, *35*, 1267–1272. [CrossRef]
3. Brenner, A. *Electrodeposition of Alloys: PRINCIPLES and PRACTICE*; Elsevier: Amsterdam, The Netherlands, 1963.
4. Eliaz, N.; Venkatakrishna, K.; Hegde, A.C. Electroplating and Characterization of Zn–Ni, Zn–Co and Zn–Ni–Co Alloys. *Surf. Coat. Technol.* **2010**, *205*, 1969–1978. [CrossRef]

5. Cao, F.; Wang, J.; Lian, Y.; Wang, Y.; Wang, X.; Wang, X.; Song, A.; Shi, L. A Study on the Influence of the Electroplating Process on the Corrosion Resistance of Zinc-Based Alloy Coatings. *Coatings* **2023**, *13*, 1774. [CrossRef]
6. Riđošić, M.; García-Lecina, E.; Salicio-Paz, A.; Bajat, J. The Advantage of Ultrasound during Electrodeposition on Morphology and Corrosion Stability of Zn-Co Alloy Coatings. *Trans. IMF* **2020**, *98*, 114–120. [CrossRef]
7. Anwar, S. Electrochemical and Corrosion Behavior of Electrodeposited Zn, Zn-Ni Alloy and Zn-Ni-TiO_2 Composite Coatings. Ph.D. Thesis, Memorial University of Newfoundland, St. John's, NL, Canada, 2020.
8. Soleimangoli, F.; Hosseini, S.A.; Davoodi, A.; Alishahi, M. Quantitative Power Spectral Density Analysis of Nano/Microstructured Ni-Zn Electrodeposit and Its Correlation with Superhydrophobicity. *Thin Solid Film* **2023**, *779*, 139917. [CrossRef]
9. Singh, R.; Arab, A.; Caceres, A.; Eybel, R.; Medraj, M. Establishing Industrial Zn Ni Brush Electroplating Process without Post-Plating Hydrogen Embrittlement Relief Baking. *Surf. Coat. Technol.* **2024**, *478*, 130363. [CrossRef]
10. Mosavat, S.H.; Shariat, M.H.; Bahrololoom, M.E. Study of Corrosion Performance of Electrodeposited Nanocrystalline Zn–Ni Alloy Coatings. *Corros. Sci.* **2012**, *59*, 81–87. [CrossRef]
11. Byk, T.V.; Gaevskaya, T.V.; Tsybulskaya, L.S. Effect of Electrodeposition Conditions on the Composition, Microstructure, and Corrosion Resistance of Zn–Ni Alloy Coatings. *Surf. Coat. Technol.* **2008**, *202*, 5817–5823. [CrossRef]
12. Hammami, O.; Dhouibi, L.; Triki, E. Influence of Zn–Ni Alloy Electrodeposition Techniques on the Coating Corrosion Behaviour in Chloride Solution. *Surf. Coat. Technol.* **2009**, *203*, 2863–2870. [CrossRef]
13. Hammami, O.; Dhouibi, L.; Berçot, P.; Rezrazi, E.M.; Triki, E. Study of Zn-Ni Alloy Coatings Modified by Nano-SiO_2 Particles Incorporation. *Int. J. Corros.* **2012**, *2012*, 301392. [CrossRef]
14. Tuaweri, T.J.; Jombo, P.P.; Okpala, A.N. Corrosion Resistance Characteristics of Zn-Ni/SiO_2 Composite Coatings. *Deleted J.* **2014**, *3*, 1–12.
15. Kwon, M.; Jo, D.; Cho, S.H.; Kim, H.T.; Park, J.-T.; Park, J.M. Characterization of the Influence of Ni Content on the Corrosion Resistance of Electrodeposited Zn–Ni Alloy Coatings. *Surf. Coat. Technol.* **2016**, *288*, 163–170. [CrossRef]
16. Feng, Z.; Li, Q.; Zhang, J.; Yang, P.; An, M. Electrochemical Behaviors and Properties of Zn-Ni Alloys Obtained from Alkaline Non-Cyanide Bath Using 5,5′-Dimethylhydantoin as Complexing Agent. *J. Electrochem. Soc.* **2015**, *162*, D412–D422. [CrossRef]
17. Yang, Y.; Bian, Y.; Gao, Q.; Dong, S.; Ma, R.; Fan, Y.; Du, A.; Zhao, X.; Yang, M.; Cao, X. Corrosion Resistance Study of Zn-Ni-B4C Composite Superhydrophobic Coatings with Hierarchical Rough Structure. *Appl. Surf. Sci.* **2023**, *622*, 156882. [CrossRef]
18. Nhiem, L.T.; Oanh, D.T.Y.; Hieu, N.H. Nanocoating toward Anti-corrosion: A Review. *Vietnam. J. Chem.* **2023**, *61*, 284–293. [CrossRef]
19. Abdeen, D.H.; Hachach, M.E.; Koc, M.; Atieh, M.A. A Review on the Corrosion Behaviour of Nanocoatings on Metallic Substrates. *Materials* **2019**, *12*, 210. [CrossRef]
20. Aliofkhazraei, M.; Walsh, F.C.; Zangari, G.; Köçkar, H.; Alper, M.; Rizal, C.; Magagnin, L.; Protsenko, V.; Arunachalam, R.; Rezvanian, A.; et al. Development of Electrodeposited Multilayer Coatings: A Review of Fabrication, Microstructure, Properties and Applications. *Appl. Surf. Sci. Adv.* **2021**, *6*, 100141. [CrossRef]
21. Sadreddini, S.; Salehi, Z.; Rassaie, H. Characterization of Ni–P–SiO_2 Nano-Composite Coating on Magnesium. *Appl. Surf. Sci.* **2014**, *324*, 393–398. [CrossRef]
22. Silviana, S.; Lukmilayani, C. Metal Coatings Derived from Modified Silica as Anti-Corrosion. *Defect Diffus. Forum* **2024**, *431*, 77–95. [CrossRef]
23. Sadreddini, S.; Afshar, A. Corrosion Resistance Enhancement of Ni-P-Nano SiO_2 Composite Coatings on Aluminum. *Appl. Surf. Sci.* **2014**, *303*, 125–130. [CrossRef]
24. Li, R.; Hou, Y.; Liang, J. Electro-Codeposition of Ni-SiO_2 Nanocomposite Coatings from Deep Eutectic Solvent with Improved Corrosion Resistance. *Appl. Surf. Sci.* **2016**, *367*, 449–458. [CrossRef]
25. Jiang, W.; Huang, M.; Lao, Y.; Yang, X.; Wang, C.; Tian, Z.; Zhou, S.; Mutschke, G.; Eckert, K. Experimental and Numerical Investigations of Ni–Co–SiO_2 Alloy Films Deposited by Magnetic-Field-Assisted Jet Plating. *Surf. Coat. Technol.* **2021**, *423*, 127583. [CrossRef]
26. Ramanauskas, R.; Gudavičiūtė, L.; Juškėnas, R.; Ščit, O. Structural and Corrosion Characterization of Pulse Plated Nanocrystalline Zinc Coatings. *Electrochim. Acta* **2007**, *53*, 1801–1810. [CrossRef]
27. Ullal, Y.; Hegde, A.C. Corrosion Protection of Electrodeposited Multilayer Nanocomposite Zn-Ni-SiO_2 Coatings. *Surf. Engin. Appl. Electrochem.* **2013**, *49*, 161–167. [CrossRef]
28. Li, R.; Hou, Y.; Liu, B.; Wang, D.; Liang, J. Electrodeposition of Homogenous Ni/SiO_2 Nanocomposite Coatings from Deep Eutectic Solvent with in-Situ Synthesized SiO_2 Nanoparticles. *Electrochim. Acta* **2016**, *222*, 1272–1280. [CrossRef]
29. Zhang, X.; Xiong, S.; Gao, F.; Du, J.; Du, Q.-J. Preparation and Tribological Properties of SiO_2 /WO_3 Nanocomposite Lubricant. *Ind. Lubr. Tribol.* **2022**, *75*, 60–66. [CrossRef]
30. Alekseeva, M.V.; Gulyaeva, Y.K.; Bulavchenko, O.A.; Saraev, A.A.; Kremneva, A.M.; Stepanenko, S.A.; Koskin, A.P.; Kaichev, V.V.; Yakovlev, V.A. Promoting Effect of Zn in High-Loading Zn/Ni-SiO_2 Catalysts for Selective Hydrogen Evolution from Methylcyclohexane. *Dalton Trans.* **2022**, *51*, 6068–6085. [CrossRef]

31. Xiang, T.; Zhang, M.; Li, C.; Dong, C.; Yang, L.; Chan, W. CeO_2 Modified SiO_2 Acted as Additive in Electrodeposition of Zn-Ni Alloy Coating with Enhanced Corrosion Resistance. *J. Alloy. Compd.* **2017**, *736*, 62–70. [CrossRef]
32. Karunarathne, V.K.; Paul, S.C.; Šavija, B. Development of Nano-SiO_2 and Bentonite-Based Mortars for Corrosion Protection of Reinforcing Steel. *Materials* **2019**, *12*, 2622. [CrossRef]
33. Tu, W.-Y.; Xu, B.-S.; Dong, S.-Y.; Wang, H. Electrocatalytic Action of Nano-SiO_2 with Electrodeposited Nickel Matrix. *Mater. Lett.* **2005**, *60*, 1247–1250. [CrossRef]
34. Silva-Alvarez, D.F.; Dominguez-Lopez, I.; Hurtado, M.A.V.; Gutierrez-Antonio, C.; Flores-Garay, K.A.; Garcia-Garcia, A.L. A Review on the Menagerie of Green Fluids and Nanoparticles to Develop Sustainable Biolubricant Technologies. *Environ. Technol. Innov.* **2024**, *33*, 103532. [CrossRef]
35. Hou, C.; Fan, Z.; Yang, J. Construction of Super Hydrophobic Paper by Modified Nano-SiO_2 Hybrid Medium Fluoro-Epoxy Polymer and Its Properties. *Prog. Org. Coat.* **2024**, *187*, 108180. [CrossRef]
36. Xiong, Z.; Chen, N.; Wang, Q. Preparation and Properties of Melamine Formaldehyde Resin Modified by Functionalized Nano-SiO_2 and Polyvinyl Alcohol. *Polym. Polym. Compos.* **2020**, *29*, 96–106. [CrossRef]
37. Hu, M.; Liu, M.; Li, P.; Du, J.; Yu, Y.; Guo, J. Effects of Triethanolamine Modified Graphene Oxide on Calcium Silicate Hydrate in Synthesized System and Cement Composite. *Colloid Surf. Physicochem. Eng. Asp.* **2020**, *602*, 125037. [CrossRef]
38. Kelly, R.G.; Scully, J.R.; Shoesmith, D.W. *Electrochemical Techniques in Corrosion Science and Engineering*; CRC Press: Boca Raton, FL, USA, 2003.
39. Bonin, L.; Vitry, V.; Delaunois, F. Inorganic Salts Stabilizers Effect in Electroless Nickel-Boron Plating: Stabilization Mechanism and Microstructure Modification. *Surf. Coat. Technol.* **2020**, *401*, 126276. [CrossRef]
40. *ASTM G5-14*; Standard Reference Test Method for Making Potentiodynamic Anodic Polarization Measurements. ASTM International: West Conshohocken, PA, USA, 2021. [CrossRef]
41. *ASTM G106-89*; Standard Practice for Verification of Algorithm and Equipment Used for Electrochemical Impedance Measurements. ASTM International: West Conshohocken, PA, USA, 2015.
42. *ASTM B117-20*; Standard Practice for Operating Salt Spray (Fog) Apparatus. ASTM International: West Conshohocken, PA, USA, 2020.